NASA Technical Memorandum 87255

Evaluation of a Hybrid Hydrostatic Bearing for Cryogenic Turbopump Application

Paul W. Spica, Ned P. Hannum,
and Scott D. Meyer
Lewis Research Center
Cleveland, Ohio

April 1986

NASA

EVALUATION OF A HYBRID HYDROSTATIC BEARING FOR CRYOGENIC TURBOPUMP APPLICATION

Paul W. Spica, Ned P. Hannum, and Scott D. Meyer
National Aeronautics and Space Administration
Lewis Research Center
Cleveland, Ohio 44135

SUMMARY

A hybrid hydrostatic bearing was designed to operate in liquid hydrogen at speeds to 80 000 rpm and radial loads to 440 N (100 lbf). The bearing assembly consisted of a pair of 20-mm angular-contact ball bearings encased in a journal, which was in turn supported by a fluid film of liquid hydrogen. The size and operating conditions of the bearing were selected to be compatible with the operating requirements of an advanced technology turbopump.

Several test parameters were varied to characterize the bearing's steady-state operation. The rotation of the tester shaft was varied between 0 and 80 000 rpm. Bearing inlet fluid pressure was varied between 2.07 and 4.48 MPa (300 and 650 psia), while the fluid sump pressure was independently varied between 0.34 and 2.07 MPa (50 and 300 psia). The maximum radial load applied to the bearing was 440 N (100 lbf).

Measured hybrid-hydrostatic-bearing stiffness was 1.5 times greater than predicted, while the fluid flow rate through the bearing was 35 to 65 percent less than predicted. Under two-phase fluid conditions, the stiffness was even greater and the flow rate was less. The optimal pressure ratio for the bearing should be between 0.2 and 0.55 depending on the balance desired between bearing efficiency and stiffness. Startup and shutdown cyclic tests were conducted to demonstrate the ability of the hybrid-hydrostatic-bearing assembly to survive at least a 300-firing-duty cycle. For a typical cycle, the shaft was accelerated to 50 000 rpm in 1.8 sec. The bearing operated for 337 start-stop cycles without failure.

INTRODUCTION

Rolling-element bearings run in cryogenic environments are usually lubricated by a solid film of Teflon, which is transferred from the bearing cage to the rolling elements and then to the bearing raceways (ref. 1). When this film can no longer be replenished, bearing failure due to excessive wear of the cage, rolling elements, and/or raceways generally results. Hence, wear is the limiting phenomena to long-life rolling-element bearings in this application.

Angular-contact ball bearings are used in the space shuttle main engine (SSME) turbopump. Because of wear, the bearings are generally replaced after three missions or after approximately 1500 sec of operation. Bearing life can be extended by replacing the rolling-element bearings with fluid-film bearings (ref. 2).

The objective of this report is to evaluate a hybrid hydrostatic bearing for cryogenic turbopump applications. The hybrid hydrostatic bearing tested

consisted of a pair of 20-mm angular-contact ball bearings encased in a journal, which in turn was supported by a fluid film. The purpose of the ball bearings was to prevent wear of the journal and of the hydrostatic bearing prior to pressurization at startup and during shutdown of the system. The size of the bearing and the operating conditions were selected to be compatible with the operating requirements of an advanced technology turbopump. Liquid hydrogen was used as the working fluid with speeds to 80 000 rpm and radial loads to 440 N (100 lbf). Startup and shutdown cyclic tests were also conducted.

SYMBOLS

BN	bearing number, Re/GRADP
C	hydrostatic-bearing radial clearance, mm (in.)
D_S	hydrostatic-bearing surface diameter, mm (in.)
E	eccentricity ratio, e/C
e	eccentricity or journal deflection, mm (in.)
GRADP	modified Reynolds number based on axial pressure flow, $(GRADPS)(PR)D_S/(L - w)$
GRADPS	Reynolds number based on axial pressure flow, $(P_S - P_a)C^3/R(\mu)\upsilon$
K	static stiffness, N/cm (lbf/in.)
$\overline{K}$	dimensionless stiffness, $K(C)/(P_S - P_a)L(D_S)$
L	journal axial length, mm (in.)
LOFLO	load-to-flow ratio, $W(C^4)/e(m)\upsilon(L)D_S$
m	mass flow rate through the hydrostatic bearing, g/sec (lbm/sec)
PR	pocket pressure ratio, $(P_r - P_a)/P_S - P_a)$
P_a	sump pressure, MPa (psia)
P_r	pocket pressure, MPa (psia)
P_S	bearing inlet pressure, MPa (psia)
R	radius of the hydrostatic bearing, mm (in.)
Re	Reynolds number, U(C)/2
U	journal surface velocity, mm/sec (in./sec)
W	load applied to the bearing, N (lbf)

$\bar{W}$ dimensionless load, $W/(P_s - P_a)L(D_s)$

w axial length of pocket, mm (in.)

θ attitude angle, deg

μ inlet fluid viscosity, N sec/mm^2 (lbf sec/in.^{2})

ν inlet fluid kinematic viscosity, mm^2/sec (in.^{2}/sec)

APPARATUS

Test Bearing

A schematic of the hybrid-hydrostatic-bearing assembly and its design details are shown in figure 1. Design details of the hybrid hydrostatic bearing were reported in reference 3. Table I contains critical dimensions of the two hydrostatic-bearing configurations tested. Fabrication of two sets of hardware resulted in some dimensional differences, mainly affecting the clearance between the journal and the hydrostatic bearing surface. Liquid hydrogen was supplied to the hydrostatic bearing through twenty orifice-compensated pockets that were arranged in two staggered rows of ten equally spaced pockets. The rolling element of the hybrid bearing consisted of two angular-contact, 20-mm-bore ball bearings. The ball bearings, which were preloaded by a spring washer, act at system startup and shutdown to prevent wear of the hydrostatic bearing and at system startup to prevent high-friction torque.

The clearance between the journal and the hydrostatic bearing surface is a critical design parameter for determining the stiffness of and the fluid flow through a hydrostatic bearing. The value of the fluid-film clearance at room temperature and zero rotational speed changes when the hybrid bearing is operating at liquid-hydrogen temperatures and high speed depending on the materials involved. Inconel 718 with a thin, dense chrome plating was used for the journal material, and 316 stainless steel with an electro-deposited silver plating was used for the hydrostatic bearing. When thermal-expansion coefficients were used for these materials, calculations indicated that a temperature decrease from ambient to 21 K (37 °R) resulted in a 0.01-mm (0.0004-in.) decrease in the radial clearance. A finite-element analysis was used to calculate the growth of the journal due to fluid pressure and centrifugal forces. The 0.066 mm (0.0026 in.) radial clearance of the hydrostatic bearing at ambient conditions was reduced to 0.035 mm (0.0014 in.) at an operating temperature of 21 K (37 °R), a speed of 90 000 rpm, and a pressure of 1.7 MPa (250 psia).

Test Rig

Figure 2 shows the hybrid hydrostatic-bearing test assembly used in this investigation. It consisted of a horizontal shaft supported at both ends by hybrid hydrostatic bearings driven by an overhung turbine. Axial-shaft loads were supported by a hydrostatic thrust bearing while the radial loads were supported by two test hybrid hydrostatic bearings. Radial loads were applied at the shaft center by a radial-loading piston.

A schematic of the bearing tester is shown in figure 3. Liquid hydrogen was supplied independently to each hybrid bearing through passages in the housing and was removed from the tester through a common drain. This drain flow was throttled to generate back pressure in the hybrid-bearing tester to prevent fluid boiling. A portion of the hydrostatic-bearing flow was returned to the tester sump after passing through the ball bearings to cool them. The turbine had a radial inflow design with cantilevered blades driven by ambient-temperature hydrogen gas. This turbine was designed for speeds up to 120 000 rpm and could deliver up to 12 kW (16.2 hp) of power. Sufficient torque was developed to accelerate the shaft up to 50 000 rpm/sec.

The radial-loading piston consisted of a hydrostatic bearing acting over a partial arc of the shaft. Radial loads were developed by the hydrostatic pressure acting over the area of the bearing foot. Up to 880 N (200 lbf) could be applied to the tester shaft center (440 N (100 lbf) per hybrid hydrostatic bearing).

Strain-gauge pressure transducers were used to measure fluid pressures in the tester and in the fluid lines leading to the tester. Temperatures were measured using platinum resistance thermometers. Flow rates through the hydrostatic elements were measured by venturi flowmeters. Other flow rates were measured by turbine flowmeters. Rotating speeds of the shaft and the journal were measured using eddy-current and optical displacement probes that detected the passage of notches or flats on the rotating parts. Data from the various transducers were recorded by a minicomputer-controlled, digital data-acquisition system. The hybrid hydrostatic bearing on the free end of the test rig was instrumented to monitor its motion with two orthogonally mounted eddy-current displacement probes that penetrated the test rig and viewed the journal.

A displacement-probe calibration at operating temperatures was obtained by using a notch (machined to a known depth) on the journal. The notch passed under both probes once every cartridge revolution. Room-temperature calibrations were made by moving the journal a measured amount while recording displacement-probe output and then rotating the notch past the probe position. This verified that the notch technique was valid and it also checked the linearity of the measurement system. Signal-conditioning electronics compensated for the voltage shifts due to the extreme temperature variations. Since journal movements as small as 0.003 mm (0.0001 in.) could be detected and measured using this measurement system, hydrostatic-bearing stiffness calculations could be made.

PROCEDURE

Assembly and Pretest

The shaft assembly was balanced in three steps. First, the hydrostatic-bearing journals were balanced individually. Next, the shaft was completely assembled and then balanced while rotating on the ball bearings. Finally, the balance of the shaft assembly was checked by allowing the journals to rotate on rollers in the balancing machine. Because the position of the journal is not constant with respect to the shaft, there is a range of values for balancing the shaft assembly. The residual unbalance for all assemblies of the shaft was less than 0.36 g/cm (0.005 oz/in.). The balance was checked each time new parts were added to the shaft assembly. All the tester parts were cleaned

ultrasonically cleaned in alcohol prior to assembly, and they were assembled in a clean-room environment to minimize particulate contamination. Once assembled, the tester was sealed to prevent damage due to condensation until it could be installed in the test facility. Each test day the installed tester and all of the associated liquid-hydrogen systems were evacuated and then purged with gaseous helium to prevent any contamination.

Prior to testing, a final evacuation of the tester was conducted. The final vacuum was broken with hydrogen gas and precooling was begun immediately. Liquid hydrogen from the storage dewar flowed to the run tank and through the tester to chill them to liquid-hydrogen temperatures. This operation typically took about 1 hr, after which the high-pressure run tank was pressurized and the final test preparations were made.

Steady-State-Characterization Tests

During the hybrid-bearing steady-state-characterization tests, the liquid-hydrogen flow to the hybrid bearings and the axial-thrust bearing was established before shaft rotation. The shaft was then accelerated to the selected test speed and the back pressures on the liquid-hydrogen drain and the turbine discharge were ramped to the selected pressures. Linear ramp generators allowed both ramp rates and ramp end points (steady operating conditions) to be set independently. Servo-operated valves were used in a closed-loop control system to regulate the various flows and pressures to the tester. Once all test conditions were established, the radial load was gradually applied while observing journal-displacement instrumentation on an oscilloscope. The displacement traces indicated the proximity to the shaft, the orbiting amplitude, and the critical speeds. If orbits were particularly large (owing to operation close to a critical speed), a relatively small radial load would deflect the bearing enough to cause a journal rub. This information was also recorded on an FM tape recorder for later detailed analysis. The deflection of the journal could be measured and the stiffness of the hydrostatic bearing could be determined by adding and then removing the radial load. After obtaining this measurement, the shaft speed or the pressure drop across the bearing was varied and the journal deflection was again measured.

Several test parameters were varied to characterize the steady-state operation of the hybrid hydrostatic bearing. The rotation of the shaft was varied between 0 and 80 000 rpm; the inlet fluid pressure to the hydrostatic bearing was varied between 2.07 and 4.48 MPa (300 and 650 psia); and the fluid sump pressure was independently varied between 0.34 and 2.07 MPa (50 and 300 psia). The maximum radial load applied to a hybrid bearing was 440 N (100 lbf).

Cyclic Tests

Start-stop cyclic tests were conducted to demonstrate the ability of the hybrid-hydrostatic-bearing assembly to survive the 300-firing-duty cycle required for turbopump application. Each time the bearing starts or stops the journal must rub against the mating bearing surface. In an actual turbopump the fluid supply to the hybrid bearings would be derived from the pumped fluid. The available fluid pressure would be dependent on the rotating speed of the pump, the pressure being approximately proportional to the pump speed squared.

In addition, any static radial-bearing loads would be derived from the pressure of the pumped fluid and would also be proportional to the pump speed squared. Thus, to simulate properly the turbopump environment during shaft-speed transients, it was necessary to control the bearing supply pressure and the radial-shaft load so that they would be proportional to the shaft speed squared. The shaft acceleration rate and radial-shaft load were selected to be typical of a turbopump of this type. The bearing supply pressures were selected to avoid operation at any of the tester critical speeds.

For a typical start-stop cycle the shaft was accelerated to 50 000 rpm in 1.8 sec. The liquid-hydrogen inlet pressure on the hybrid bearings increased in proportion to shaft speed squared until a bearing pressure drop of 1.8 MPa (260 psia) was reached. Simultaneously, the radial shaft load varied in proportion to shaft speed squared from 0 N at 0 rpm to a final value of 110 N (25 lbf) per bearing at 50 000 rpm. The liquid-hydrogen drain pressure varied in proportion to shaft speed to a final value of 0.6 MPa (80 psia). Once 50 000 rpm was reached, the shaft was decelerated to zero rotational speed. Shaft deceleration was due to windage in the hybrid bearing and turbine cavities. At low speeds, rolling friction due to ball rotation further decelerated the shaft. This cycle was repeated for a total of 337 cycles, at which time the tester was disassembled.

EFFECT OF SPEED ON RADIAL CLEARANCE AND STIFFNESS

The radial clearance of a hydrostatic bearing is defined as the radius of the hydrostatic bearing's surface minus the radius of the journal. The clearance affects the load-carrying capacity and the stiffness of the hydrostatic bearing. In turn, stiffness affects the critical speed of the rotor.

Because of journal growth due to centrifugal force effects at high speed, the operating radial clearance of the hydrostatic bearing will change. While this effect could not be directly measured, it could be calculated. The result of this calculation, under no-load conditions, is shown in figure 4 for the two bearing configurations. At cryogenic temperatures and no rotational speed, the clearances were 0.069 and 0.066 mm (0.0027 and 0.0026 in.) for configurations 1 and 2, respectively. At 90 000 rpm these clearances decreased to 0.043 and 0.035 mm (0.0017 and 0.0014 in.), respectively.

Hydrostatic-bearing stiffness can be defined as the static radial load applied to the hybrid bearing divided by the journal deflection. This value is plotted against radial clearance in figure 5. Configuration and speed do not effect stiffness except in relation to their effect on radial clearance. The vertical lines indicate the uncertainty in the stiffness calculation due to the accuracy limitations of the journal deflection measurements. The boundaries of the vertical lines represent ±0.0013 mm (±0.00005 in.) of measured journal movement. These data indicate that, for the hydrostatic bearing investigated,

$$\text{Stiffness (in N/cm)} = 8.91\times10^{5} - 1.07\times10^{8}\ C \qquad (C \text{ in cm})$$

$$\text{Stiffness (in lbf/in.)} = 5.05\times10^{5} - 1.544\times10^{8}\ C \qquad (C \text{ in in.})$$

Figure 6 illustrates how the hydrostatic-bearing stiffness increases when the radial clearance is coupled to the journal's rotational speed through the

journal's centrifugal growth. As the journal expands because of centrifugal growth, the radial clearance decreases, which in turn raises the hydrostatic-bearing stiffness. This changing stiffness also impacts the critical speed of the rotor system. Increasing the pressure drop across the bearing increased its stiffness. But, varying the sump pressures from 1.03 to 1.90 MPa (150 to 275 psia) while maintaining a constant total pressure drop across the hydrostatic bearing had no effect on the stiffness. The rotor's critical speed increased with bearing stiffness and, hence, with decreased radial clearance and increased pressure drop.

COMPARISON OF PREDICTED AND EXPERIMENTAL OPERATING CHARACTERISTICS

The eccentricity e of a hybrid hydrostatic bearing can be defined as the distance between the journal's center of rotation and the center of the hydrostatic bearing. Eccentricity ratio E is defined as the ratio of eccentricity to radial clearance C:

$$E = \frac{e}{C}$$

When the eccentricity ratio is equal to 1, contact between journal and hydrostatic-bearing surfaces will occur. The relation between eccentricity ratio and the load and speed of the bearing is shown in figure 7.

Figure 8 shows the bearing's dimensionless stiffness as a function of its pressure ratio. The experimental values were approximately 1.5 times the predicted values. This would result in a different rotor-dynamic performance because the critical speeds would be higher than those calculated from the predicted bearing stiffness. The two-phase-flow data points in figure 8 were recorded when the sump pressure was less than 1.03 MPa (150 psia) and the fluid-inlet temperature was less than 33 K (60 °R). Since the critical temperature and pressure for liquid hydrogen are 32.7 K and 1.30 MPa (58.9 °R and 188 psia), the increase in stiffness may be caused by fluid cavitation.

Reduced flow rates for the two-phase-flow conditions were also observed. The phenomenon of increased stiffness and decreased flow has also been observed in face seals (ref. 4).

A measure of hydrostatic-bearing effectiveness is the ratio of its load-carrying capacity to fluid-mass flow rate. This ratio, which is the amount of load-per-unit-mass flow rate through the hydrostatic bearing, is shown in figure 9 as a function of pressure ratio. The peak value of the ratio occurs at a pressure ratio of 0.2; this compares to a predicted value of 0.375. Figure 8 shows that both experimental and predicted maximum stiffness occur at a pressure ratio of 0.55. In operation the pressure ratio selected should be between 0.2 and 0.55 for optimum performance depending on the balance desired between bearing efficiency and stiffness.

Bearing number BN is the ratio of the Reynolds numbers for the circumferential and axial flows. The effect of bearing number on the journal attitude angle θ is shown in figure 10. Attitude angle is the angle between the applied radial load and the reacted load that is normal to the bearing surface. Increasing the rotational speed of the journal increases the bearing number, while increasing the flow through the hydrostatic bearing decreases

the bearing number. Increasing the bearing number also increases the attitude angle.

A comparison between the measured and predicted flow rates through the bearing is shown in figure 11 as a function of the bearing number. As the bearing number increases, the actual flow rate decreases relative to the predicted flow rate. At a bearing number of 0.002, the measured flow rate is approximately 70 percent of the predicted value. At a bearing number of 0.006, the flow rate is approximately 45 percent of the predicted value.

CYCLIC LIFE TESTS

In addition to the steady-state tests discussed previously, 337 start-stop cycles were made to determine the life characteristics of the hybrid hydrostatic bearing under simulated turbopump operating conditions. There were no intermediate tear downs of the hardware and no failures occurred. Series of up to 26 start-stop transient cycles, similar to the two shown in figure 12, were run. The number of cycles in a series was limited by the computer storage capacity. As shown in figure 12, the journal speed lags the shaft speed during the start and at times during the stop transients. This means that the ball bearings will sometimes reverse their rotational direction. All cyclic tests were extended until the shaft and journal speed were equal.

Figure 13 shows that the degree to which the journal speed lags the shaft speed is a function of the shaft acceleration rate. This indicates that the lag is more an effect of inertia than of rubbing. Sudden changes in the speed would indicate that rubbing was occurring. Displacement data indicate that in the simulated-turbopump start transients, the journal lifts before there is any appreciable journal-rotation rubbing. Observation of the journal speed as a function of time during the stop transients, however, shows some quick stops, which indicate rubbing of the journal.

SUMMARY OF RESULTS

A hybrid hydrostatic bearing was designed to operate in liquid hydrogen at speeds to 80 000 rpm and static radial loads to 440 N (100 lbf). The hybrid-hydrostatic-bearing assembly consisted of a pair of 20-mm ball bearings encased in a journal, which was in turn supported by a fluid film of liquid hydrogen. The size and operating conditions of the bearing were selected to be compatible with the operating requirements of an advanced technology turbopump. The following results were obtained:

1. The hybrid hydrostatic bearing operated for 337 cyclic tests in hydrogen under simulated turbopump conditions without failure.

2. Measured fluid flow through the bearing was 35 to 55 percent less than predicted.

3. Calculated bearing stiffness was 1.5 times greater than that predicted using cryogenic liquid. Under two-phase fluid conditions, bearing stiffness increased even further.

4. The optimal pressure ratio for the bearing should be between 0.2 and 0.55, depending on the balance desired between efficiency and stiffness.

REFERENCES

1. Scibbe, H.W.; Brewe, D. E.; and Coe, H. H.: Lubrication and Wear of Ball Bearings in Cryogenic Hydrogen. NASA TM X-52476, 1968.

2. Young, W.E.; and Reddecliff, J. M.: Investigation of Hydrostatic Bearings for Use in High Pressure Cryogenic Turbopumps. AFRPL-TR-67-130, Air Force Rocket Propulsion Lab, May 1967.

3. Winn, L.W.; Eusepi, M.W.; and Smalley, A.J.: Small, High Speed Bearing Technology for Cryogenic Turbopumps. (MTI-74TR29, Mechanical Technology Inc.; NASA Contract NAS3-17773) NASA CR-134615, 1974.

4. Lebeck, A.O.: A Mixed Friction Hydrostatic Face Seal Model With Phase Change. J. Lubr. Technol., vol. 102, no. 2, Apr. 1980, pp. 133-138.

TABLE I. - CRITICAL HYDROSTATIC DIMENSIONS

[Number of pockets per row, 10; number of rows, 2.]

(a) Common dimensions for configurations 1 and 2

Description	Nominal dimensions	
	mm	in.
Journal axial length, L	23.5	0.926
Pocket axial length, w	2.3	.091
Pocket circumferential length, ℓ	5.9	.232
Axial land length, X	6.0	.236
Pocket depth (max.), d	.56	.022
Orifice diameter, d_o	.66	.026
Orifice length, Y	1.1	.045

(b) Dimensional differences between configurations 1 and 2

Description[a]	Configuration 1		Configuration 2	
	mm	in.	mm	in.
Journal diameter, D_J	41.76	1.6440	43.83	1.7255
Hydrostatic-bearing surface diameter, D_S	41.90	1.6497	43.96	1.7306
Diametrical clearance, $D_J - D_S$	.14	.0057	.13	.0051

[a]At ambient conditions and 0 rpm.

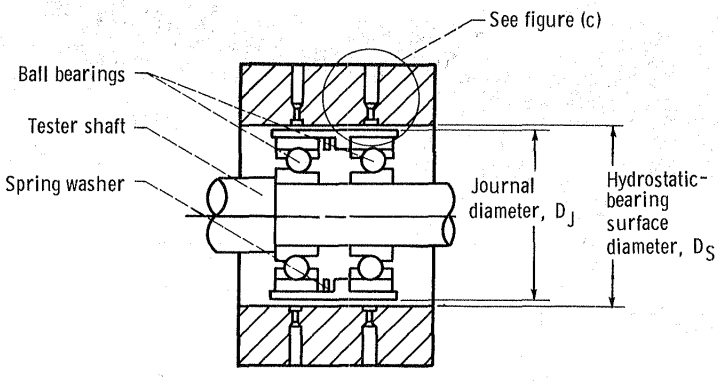

(a) Assembly schematic.

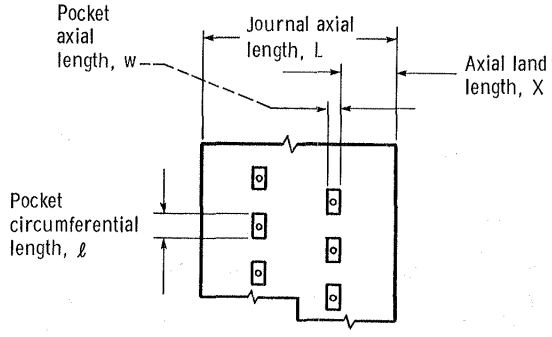

(b) Hydrostatic bearing surface.

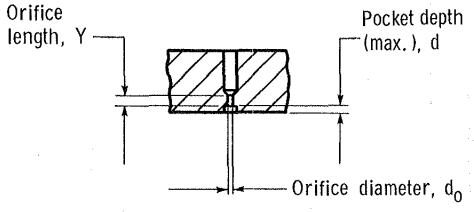

(c) Orifice details.

Figure 1. - Hybrid hydrostatic bearing. (Critical hydrostatic dimensions are given in table I.)

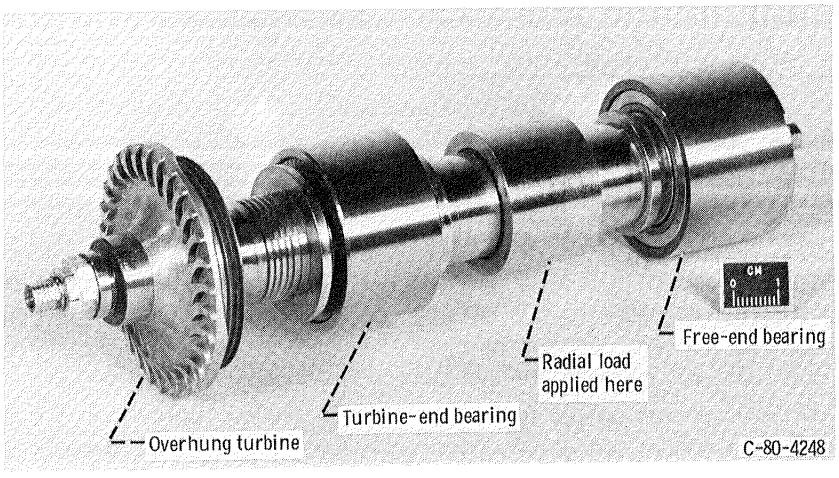

Figure 2. - Hybrid-hydrostatic-bearing test assembly.

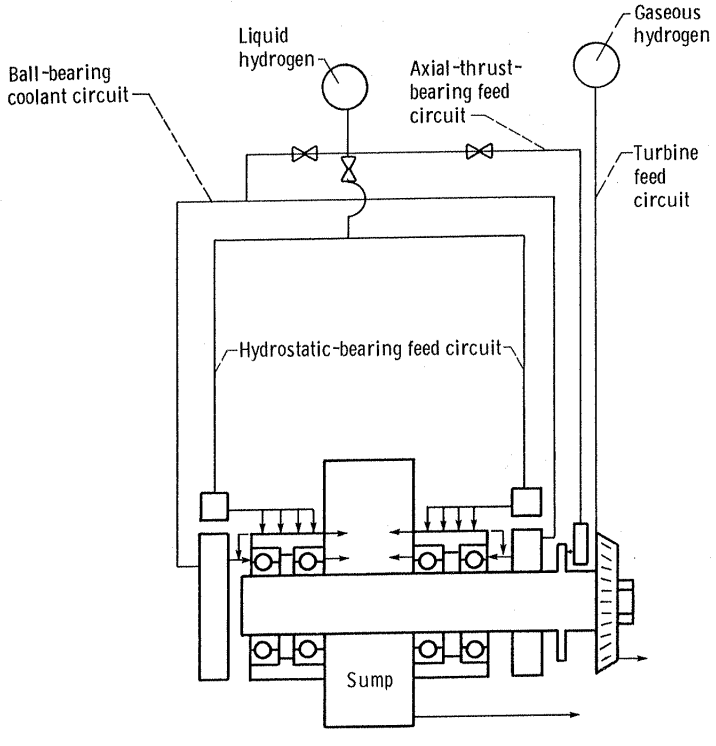

Figure 3. - Schematic of test rig.

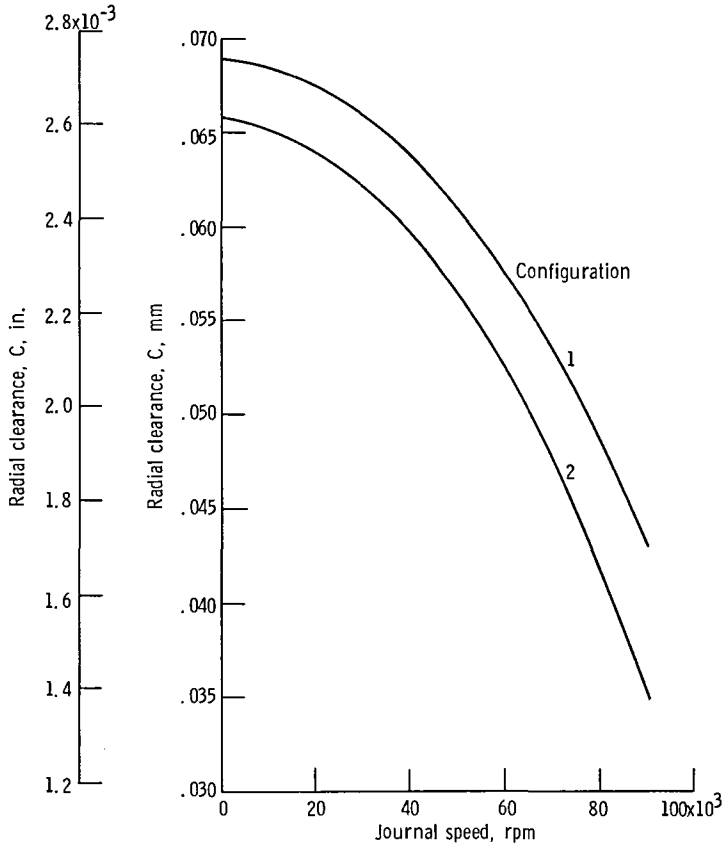

Figure 4. - Calculated effect of speed on radial clearance at cryogenic temperatures without load being applied.

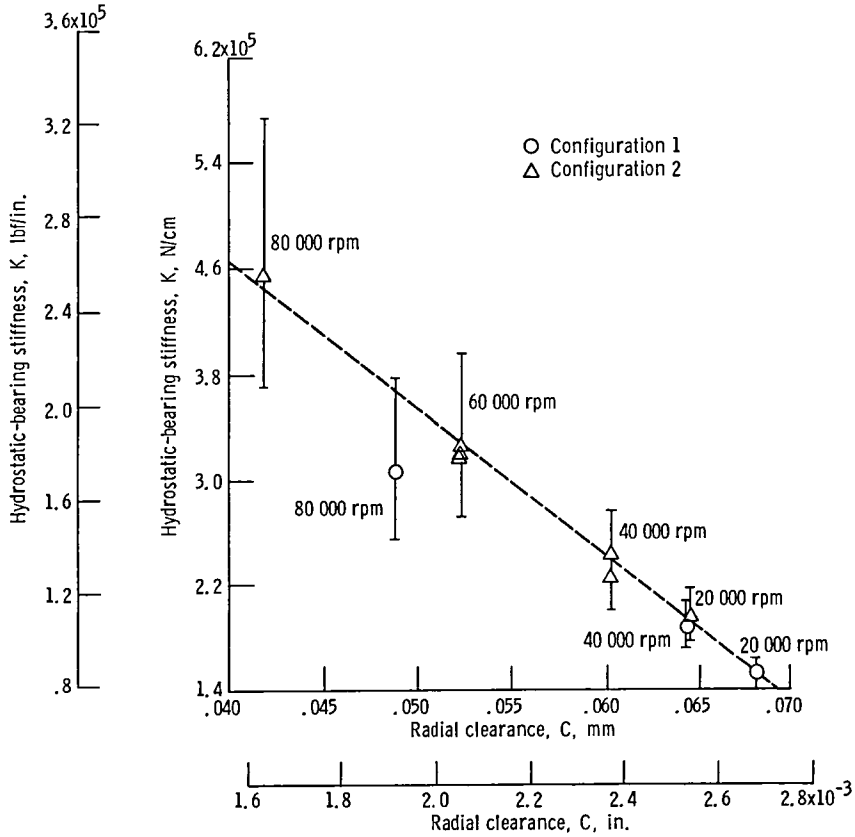

Figure 5. - Effect of hydrostatic-bearing radial clearance on hydrostatic-bearing stiffness.

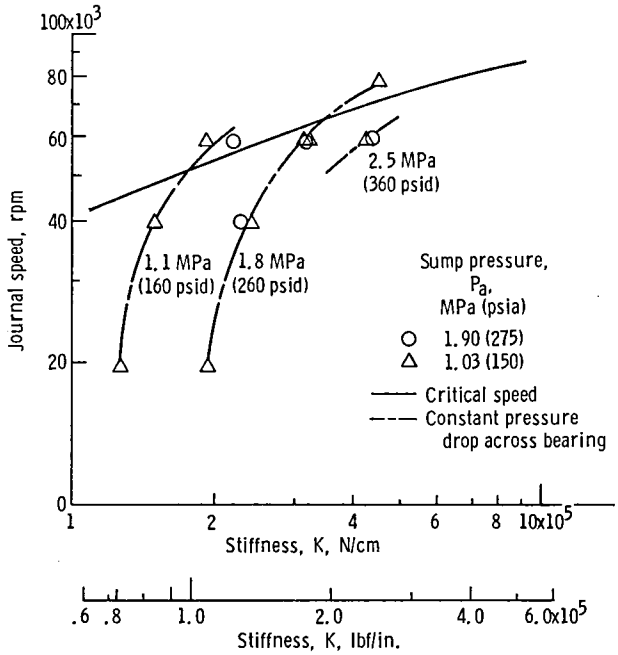

Figure 6. - Hydrostatic-bearing stiffness as function of speed and pressure drop across hydrostatic bearing.

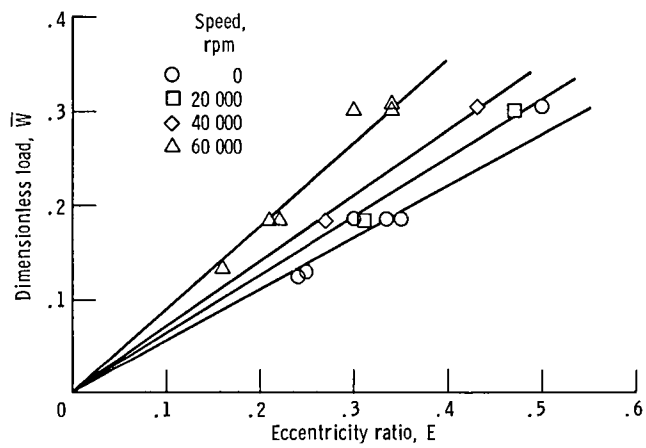

Figure 7. - Effect of load and speed on bearing eccentricity.

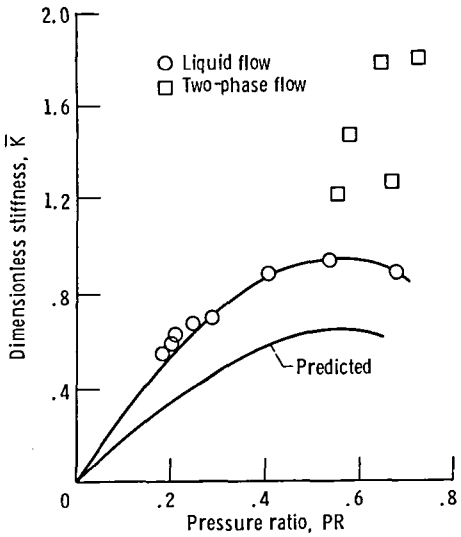

Figure 8. - Pressure-ratio effects on bearing stiffness.

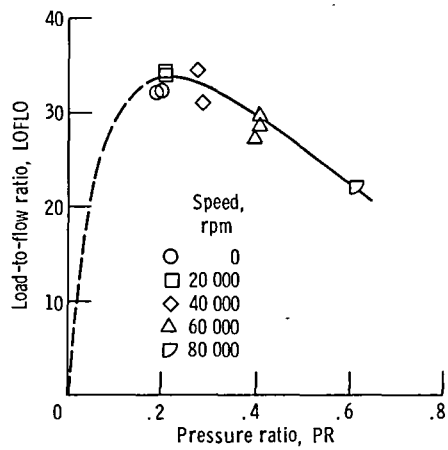

Figure 9. - Effect of pressure ratio on load-to-flow ratio. Configuration 2; total pressure drop ($P_s - P_a$) = 1.8 MPa (260 psia).

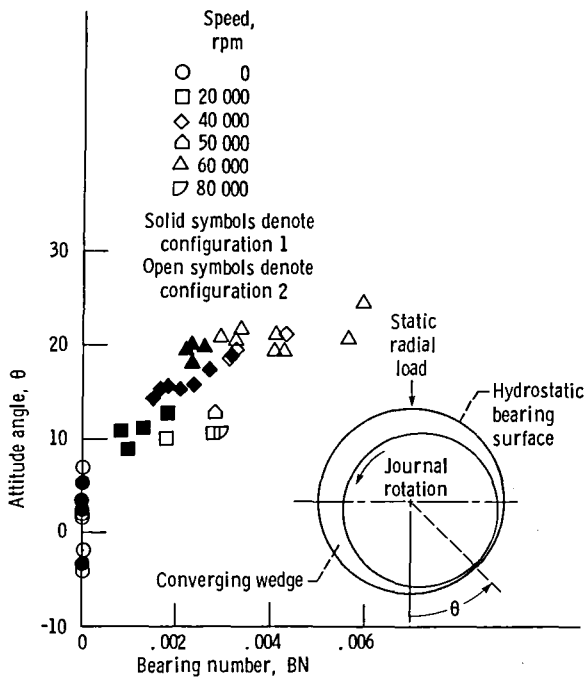

Figure 10. - Effect of bearing number on journal attitude angle.

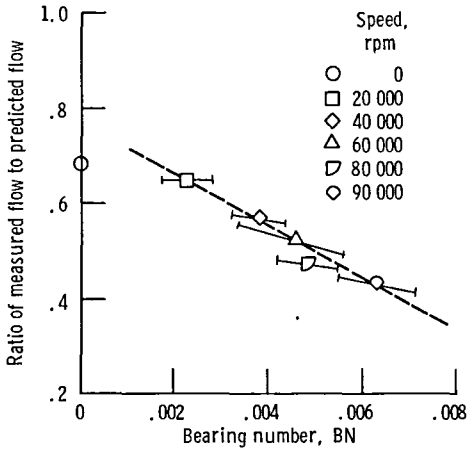

Figure 11. - Experimental and predicted flow rates for various bearing numbers for configuration 2.

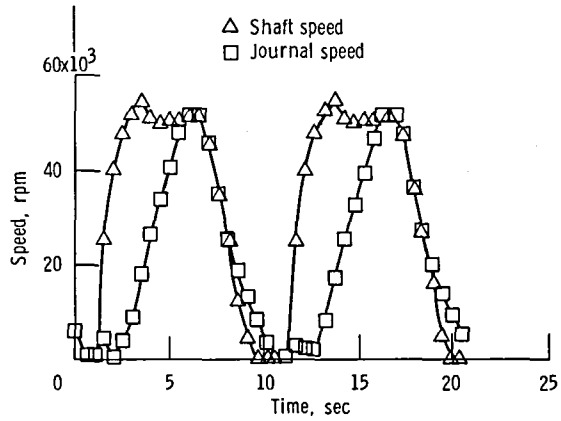

Figure 12. - Typical start-stop cycle of shaft and journal speed as function of time.

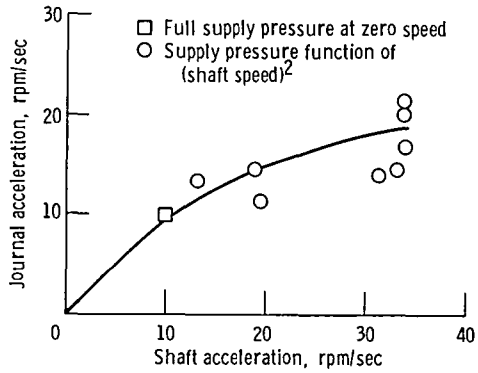

Figure 13. - Comparison of journal and shaft acceleration rates.

1. Report No.	2. Government Accession No.	3. Recipient's Catalog No.
NASA TM-87255		

4. Title and Subtitle	5. Report Date
Evaluation of a Hybrid Hydrostatic Bearing for Cryogenic Turbopump Application	April 1986
	6. Performing Organization Code: 506-60-42
7. Author(s): Paul W. Spica, Ned P. Hannum, and Scott D. Meyer	8. Performing Organization Report No.: E-2945
	10. Work Unit No.
9. Performing Organization Name and Address: National Aeronautics and Space Administration, Lewis Research Center, Cleveland, Ohio 44135	11. Contract or Grant No.
	13. Type of Report and Period Covered: Technical Memorandum
12. Sponsoring Agency Name and Address: National Aeronautics and Space Administration, Washington, D.C. 20546	14. Sponsoring Agency Code

15. Supplementary Notes

16. Abstract

A 20-mm hybrid hydrostatic bearing was evaluated in liquid hydrogen at speeds to 80 000 rpm and radial loads to 440 N (100 lbf). The size and operating conditions of the bearing were selected to be compatible with the operating requirements of an advanced technology turbopump. Measured bearing stiffness was 1.5 times greater than predicted, while the fluid flow rate through the bearing was 35 to 65 percent less than predicted. The optimal pressure ratio for the bearing should be between 0.2 and 0.55 depending on the balance of bearing efficiency and stiffness. The bearing operated for 337 start-stop cycles without failure.

17. Key Words (Suggested by Author(s))	18. Distribution Statement
Cryogenic turbopump; Fluid film bearing; Cryogenic bearing; Hybrid bearing; Hydrostatic bearing; Cryogenic lubrication	Unclassified - unlimited STAR Category 20

19. Security Classif. (of this report)	20. Security Classif. (of this page)	21. No. of pages	22. Price*
Unclassified	Unclassified		

*For sale by the National Technical Information Service, Springfield, Virginia 22161

End of Document